Photocatalytic activity of polyaniline/Fe-doped TiO$_2$ composites by in situ polymerization method

Ozcan Koysuren & H. Nagehan Koysuren

Taylor & Francis
Taylor & Francis Group

Check for updates

Photocatalytic activity of polyaniline/Fe-doped TiO$_2$ composites by in situ polymerization method

Ozcan Koysuren[a] and H. Nagehan Koysuren[b]

[a]Department of Energy Engineering, Ankara University, Ankara, Turkey; [b]Department of Environmental Engineering, Ahi Evran University, Kirsehir, Turkey

ABSTRACT

This study was focused on the photocatalytic activity of polyaniline (Pani)/iron doped titanium dioxide (Fe–TiO$_2$) composites for the degradation of methylene blue as a model dye. TiO$_2$ nanoparticles were doped with iron ions (Fe) using the wet impregnation method and the doped nanoparticles were further combined with Pani via an in situ polymerization method. For comparison purposes, Pani composites were also synthesized in the presence undoped TiO$_2$. The photocatalyst and the composites were characterized by standard analytical techniques such as FTIR, XRD, SEM, EDX and UV–Vis spectroscopies. Fe–TiO$_2$ and its composites exhibited enhanced photocatalytic activity under ultraviolet light irradiation. Improved photocatalytic activity of Fe–TiO$_2$ was attributed to the dopant Fe ions hindering the recombination of the photoinduced charge carriers. Pani/Fe–TiO$_2$ composite with 30 wt.% of TiO$_2$ nanoparticles achieved 28% dye removal and the discoloration rate of methylene blue for the sample was 0.0025 min^{-1}. FTIR, XRD, SEM, EDX and UV–Vis spectroscopies supported the idea that Fe ions integrated into TiO$_2$ crystal structure and Pani composites were successfully synthesized in the presence of the photocatalyst nanoparticles. The novelty of this study was to investigate the photocatalytic activity of Pani composites, containing iron doped TiO$_2$ and to compare their results with that of Pani/TiO$_2$.

1. Introduction

Organic dyes are utilized in a broad range of industrial applications like textiles, pharmaceuticals, food products and cosmetics. The production of these industrial applications consumes a substantial amount of high quality water and discharges considerable amounts of highly colored wastewater, which means that organic dyes are frequently found in industrial wastewater.[1] Organic dyes are viewed as dangerous to the environment and the living beings in light of the fact that they can inhibit sunlight penetration into the water stream, reducing the photosynthetic reactions, and certain types of organic dyes are very poisonous and even cancer-causing.[2] Besides, they give color to wastewater, resulting to esthetic issues.[1] Hence, it is significant to remove organic dyes from the effluents to ease the water problems faced by the environment and the human beings. In the recent years, the efficient removal or degradation of organic dyes from the wastewater has gained great attention.[2] The most common techniques used to remove organic dyes from wastewater are adsorption, sedimentation, filtration, coagulation, electrocoagulation, which are among nondestructive techniques, and biodegradation, advanced oxidation processes (AOP), which are known as destructive techniques. In majority of the studies based on nondestructive techniques, organic dyes have been removed from the

wastewater using different kinds of adsorbents. The adsorbents such as clay, activated carbon and zeolite are very effective in most cases with all types of organic dyes. However, the adsorbents result new secondary waste following the dye removal and this new waste needs to removed and regenerated using expensive processes.[1] In addition, low adsorption capacity and selectivity of the current adsorbents restrict the adsorption technique.[2] On the other hand, the dye removal takes place through living organisms in biodegradation technique. Although this technique seems to be effective and successful to remove organic dyes from large volumes of highly colored wastewater at a low cost, it cannot be used to treat most textile effluents because of the toxicity of the most important dyes to the living organisms utilized in the treatment processes.[1] Also, it is very sensitive to numerous environmental factors such as pH and temperature.[3] For these situations, it is necessary to progress more effective treatment techniqeus for the removal of organic dyes. Among the possible techniques, advanced oxidation processes based on chemical or catalytic photooxidation have gained a growing interest. In these processes, very reactive and oxidizing free radicals are generated from the oxygen and the water present in the reaction medium. These radicals are capable of degrading organic dye molecules completely. Fenton process, ozonation, sonolysis, electrochemical oxidation, electrical discharges, wet air oxidation and photocatalytic oxidation have

been accepted as alternatives for the removal organic molecules from the wastewater using the oxidizing free radicals. Among the specified processes, semiconductor based photocatalytic oxidation has become an attractive choice because this treatment process can be performed under ambient conditions and most of organic pollutants can be completely decomposed to water and carbon dioxide molecules using appropriate photocatalyst. In addition, the photocatalyst remains chemically inert during the photocatalytic reactions and it can be used many times without loss of photocatalysis property.[1–3]

TiO$_2$, a semiconducting material, is one of the most studied photocatalyst because it is highly stable both in acidic and alkaline solutions. It is reusable, nontoxic, inexpensive and relatively easy to synthesize. Besides, it exhibits high photocatalytic activity. TiO$_2$ possesses a wide band gap, which lies in the UV range between 3.0 eV and 3.2 eV. Hence, UV light source is needed for the activation of TiO$_2$ photocatalyst in the removal of organic dyes from the wastewater.[4] TiO$_2$ in nanocrystalline structure is an important commercial product. Decreasing the crystallite size below 100 nm, TiO$_2$ nanoparticles show a pronounced absorption of UV light irradiation.[5] When TiO$_2$ nanoparticles are illuminated with UV light of energy more than 3 eV, electrons of the photocatalyst are excited from the valence band to the conduction band and they leave behind holes in the valence band.[6] These mobile charge carriers, electrons in the conduction band and holes in the valence band, are responsible for the generation of the oxidizing free radicals, decomposing the target organic molecules through the reduction and oxidation reactions. The photogenerated electrons migrate to the surface of the photocatalyst nanoparticles and convert surface adsorbed oxygen to the superoxide radicals. At the same time, the photogenerated holes migrate to the photocatalyst surface and change surface adsorbed water to the hydroxyl radicals. Organic dye molecules in contact with the photocatalyst surface can be decomposed into carbon dioxide and water by means of the superoxide and the hydroxyl radicals.[4,5]

The photocatalytic activity of TiO$_2$ suffers from the fast recombination of photogenerated electrons and holes, which reduces the efficiency of the photocatalytic reactions. Hence, various efforts have been done to improve the separation efficiency of photogenerated charge carriers including coupling with conducting polymer and doping with metal.[7] Doping TiO$_2$ with metal ions has exhibited the efficient technique to enhance the photocatalytic activity. Photogenerated electrons can diffuse to the photocatalyst surface and they can be easily trapped by dopant metal ions. At the same time, holes are then free to migrate to TiO$_2$ surface. In this way, the reduction and oxidation potential of the oxidizing free radicals, necessary to decompose the target organic molecules, can be improved and the recombination rate of photogenerated charge carriers can be reduced.[4] Various metal ions such as Nd[8], Zn[9], Mn, Co, Ni[10], Fe[11], Cu[12], Bi[13] and B[14] have been studied as dopant with TiO$_2$ to enhance the photocatalytic activity. Although the photocatalytic activity varies according to the dopant amount and the character, the studies illustrated that

the efficiency and the selectivity of a photocatalytic reaction can be enhanced by doping the semiconductor surface with metal ions.[6] Among various metal ions, iron has not gained great attention. Iron can be easily oxidized at room temparture and generate multiform oxides such as FeO and Fe$_2$O$_3$. The interaction of the specified multiform oxides (Fe^{+3}↔Fe^{+2}) provides additional electrons. Hence, iron as dopant is favorable to supply additional electrons to the conduction band of TiO$_2$ nanoparticles.[15] Alternatively, combining TiO$_2$ with conducting materials, possessing narrow band gap, has the potential to reduce the band gap of the photocatalyst and to suppress the recombination of photogenerated charge carriers. Conducting polymer can shift the photocatalytic response of TiO$_2$ from UV to visible region, which allows TiO$_2$ to benefit more from the sunlight.[4] There are several conducting polymers such as polyaniline[16], polypyrrole[17], poly(3,4-ethylenedioxythiophene)[18], polythiophene[19] and heteropolyacid-chitosan[20], which have been studied to improve the photocatalytic activity of TiO$_2$. The recombination of photoinduced charge carriers in TiO$_2$ has been suppressed by combining the photocatalyst with the conducting polymer in composite structure. Among the conducting polymers, polyaniline is thermally stable, highly conductive and nontoxic. Besides, it possesses a high absorption coefficient in the visible region. Polyaniline can transfer its photoinduced electrons to the conduction band of TiO$_2$ and it can accept holes from the valence band of the photocatalyst. This interaction between polyaniline and TiO$_2$ enhances the photocatalytic activity through suppressing the recombination of photoinduced charge carriers. All these properties make poyaniline a suitable candidate for the composite application.[16,21]

Although there are intensive studies on the photocatalytic activity of Pani/TiO$_2$ composites, only a few studies have been performed on the activity of iron doped TiO$_2$ nanoparticles. Dipak et al.[22] studied microwave absorption character of polyaniline composite including iron doped TiO$_2$. In a different study, Ren et al.[15] researched photoelectrochemical responses of iron doped TiO$_2$, coated with polyaniline. Besides, Li et al.[17] investigated photocatalytic activity of polypyrole composite, containing iron doped TiO$_2$. These studies revealed that iron doping improved the target properties of TiO$_2$ positively. As an alternatine to the literature, iron doping was applied to TiO$_2$ nanoparticles in this study and doped nanoparticles were immobilized within polyaniline matrix through synthesizing the conducting polymer in the presence of the photocatalyst nanoparticles. The photocatalytic activity of the prepared composites was evaluated and compared with polyaniline/TiO$_2$ composites by analyzing the photocatalytic decomposition of a model dye under UV light irradiation. There is no study in the literature on the photocatalytic activity of polyaniline composite, including iron doped TiO$_2$.

2. Experimental

2.1. Preparation of Pani/TiO$_2$ composites

Iron nitrate nonahydrate (Fe(NO$_3$)$_3$·9H$_2$O), provided from Sigma-Aldrich, was used as iron (Fe) source. TiO$_2$
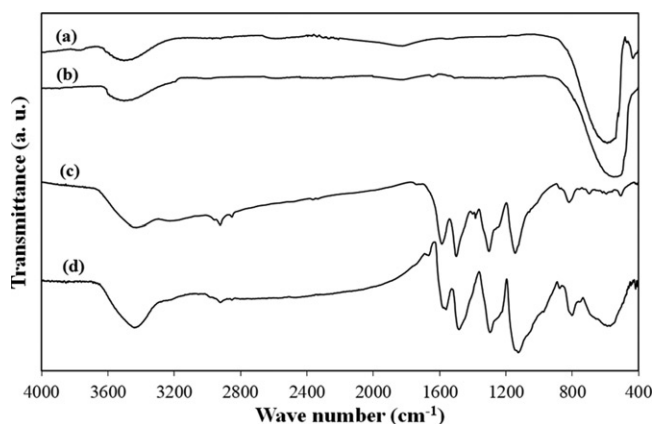
Figure 1. FTIR spectra of (a) TiO_2, (b) Fe–TiO_2, (c) Pani and (d) Pani/Fe–TiO_2 (30 wt.%).

nanoparticles (anatase, <25 nm, 99.7 trace metal basis), from Sigma-Aldrich, were used as photocatalyst. Aniline hydrochloride, ammonium peroxydisulfate, acetone and hydrochloric acid, supplied by Sigma-Aldrich, were used to synthesize the conducting polymer, polyaniline. TiO_2 nanoparticles were doped with iron though the wet impregnation method in accordance with the literature.[23,24] For this purpose, appropriate amount of $Fe(NO_3)_3 \cdot 9H_2O$ was dissolved in 100 ml of distilled water under stirring. Then 2 g of TiO_2 was added into the prepared solution and kept under stirring for 3 hours. The obtained slurry was rinsed with distilled water and dried at 100 °C for 24 hours. Finally, the dried photocatalyst was ground and calcined at 500 °C for 3 hours. The dopant content of TiO_2 nanoparticles was selected as 1 wt.%.[23,24]

Polyaniline (Pani) was synthesized in the presence of iron doped TiO_2 (Fe–TiO_2) nanoparticles via an in situ polymerization method. Aniline hydrochloride was dissolved in 100 ml of distilled water to provide 0.04 M aniline solution. Various weight ratios of Fe–TiO_2 nanoparticles were added to the 0.04 M aniline solution and kept under stirring for 1 hour. At the same time, ammonium peroxydisulfate was similarly dissolved in 100 ml of distilled water to yield 0.05 M oxidant solution. The oxidant solution was added to the aniline solution, including Fe–TiO_2 nanoparticles, drop by drop. Polymerization reaction was completed following 24 hours of stirring. The obtained slurry was rinsed with 0.2 M hydrochloric acid solution to provide more uniform doping of the conducting polymer and then with acetone for clean-up purposes. Finally, Pani/Fe–TiO_2 composite was dried at 60 °C for 24 hours.[25] Polyaniline composites, including 10, 20 and 30 wt.% Fe–TiO_2, were prepared in this way. For comparison purposes, polyaniline composites were prepared in the presence of undoped TiO_2 nanoparticles in accordance with the procedure, followed during Pani/Fe–TiO_2 synthesis. Besides, pure polyaniline was also synthesized in the absence of TiO_2 and Fe–TiO_2 nanoparticles according to the given procedure.

2.2. Methods of characterization

Fourier transform infrared (FTIR) spectra of TiO_2, Fe–TiO_2, pure Pani and Pani/Fe–TiO_2 (30 wt.%) composite were recorded by using a Nicolet 380 (Thermo Scientific) spectrophotometer in the region of 4000–400 cm^{-1}. The morphology of TiO_2, Fe–TiO_2, Pani/Fe–TiO_2 (10 wt.% and 30 wt.%) and Pani/TiO_2 (10 wt.% and 30 wt.%) was investigated by a field emission scanning electron microscope (FE-SEM, QUANTA 400F), fitted with an EDX (Energy dispersive X-ray) analyzer (JXA-8230 EDX Microanalysis Instrument). The UV–Vis absorption spectra of TiO_2, Fe–TiO_2, pure Pani, Pani/Fe–TiO_2 (30 wt.%) and Pani/TiO_2 (30 wt.%) were carried out by a Genesys 10S (Thermo Scientific) spectrophotometer in the wavelength of 200–800 nm. X-Ray diffraction (XRD) spectra of TiO_2, Fe–TiO_2 and Pani/Fe–TiO_2 (30 wt.%) were recorded over a 2Θ range from 15° to 70° on X ray diffractometer (Rigaku Ultima IV), using the Cu Kα radiation ($\lambda = 1.54$ Å).

The photocatalytic activity of TiO_2, Fe–TiO_2, pure Pani, Pani/Fe–TiO_2 (10, 20 and 30 wt.%) composites and Pani/TiO_2 (10, 20 and 30 wt.%) composites was evaluated by degradation of the model dye, methylene blue, under ultraviolet light irradiation. In a typical procedure, the wastewater was prepared from the dispersion of 10 mg/L methylene blue and 1 g/L photocatalyst. The wastewater was held in the dark for 30 minutes to provide adsorption/desorption equilibrium between the photocatalyst and the dye molecules. Then the wastewater was irradiated with a 30 W UVC lamp for another 150 minutes. Decolorization of methylene blue in wastewater was monitored by a Genesys 10S UV–VIS spectrophotometer (Thermo Scientific) at 665 nm. Before UV–visible spectroscopy, 3 ml sample of methylene blue solution was taken from the wastewater every 30 minutes and the photocatalyst was separated from the solution. The degradation of methylene blue was assessed by using the relation of C_t/C_0, where C_0 and C_t are the concentration of methylene blue initially and after treatment, respectively.[26]

3. Results and discussion

3.1. FTIR analysis

FTIR spectrum of undoped TiO_2 is shown in Figure 1a. The transmission band between 3300 cm^{-1} and 3600 cm^{-1} was attributed to the bending vibrations of water molecules adsorbed on TiO_2 nanoparticles.[23] In addition, the broad band in the range of 450 cm^{-1} to 850 cm^{-1} was related to the characteristic Ti–O–Ti stretching vibrations.[24] FTIR spectrum of Fe–TiO_2 also shows the broad transmission bands of surface adorbed water molecules and Ti–O–Ti bonds. The transmission band between 450 cm^{-1} and 850 cm^{-1} related to the Ti–O–Ti stretching moved towards the lower wavenumber region due to iron doping (Figure 1b). The intensity of this peak is more than that of the undoped photocatalyst, which might originate from the Fe-doping mechanism. By doping TiO_2 with iron, the electrons present in the $3d^6 4s^2$ level of the transition metal might absorb the photons, resulting to the increase of the band intensity.[27] Figure 1c shows FTIR spectrum of pure polyaniline. The characteristic peak of Pani related to $C = C$ stretching vibration of the quinoid rings can be seen at 1573 cm^{-1}. The transmission peak at 1492 cm^{-1} was related

to the characteristic $C=C$ stretching of the benzenoid rings. In addition, the peak at $1295\,cm^{-1}$ was corroborated to C–N stretching of tertiary aromatic amine. The transmission band in the range of $3200\,cm^{-1}$ to $3600\,cm^{-1}$ was attributed to N-H stretching vibrations of secondary amine.[28] The peaks at $1133\,cm^{-1}$ and $800\,cm^{-1}$ wavenumbers were corroborated to the electronic vibration of N quinine and C-H stretching of the benzenoid rings, respectively.[29] In general, the spectrum of the Pani/Fe–TiO$_2$ resembles to that of the pure Pani. The transmission band between $3200\,cm^{-1}$ and $3600\,cm^{-1}$ became the most prominent, which was a combined result of O–H vibrations of Fe–TiO$_2$ and N-H vibrations of Pani. Most other peaks for the pure Pani stayed in Figure 1d with small deviations due to the interaction with Fe–TiO$_2$ nanoparticles. The peaks for pure Pani at 800, 1133, 1295, 1492 and $1573\,cm^{-1}$ shifted to 792, 1112, 1286, 1469 and $1554\,cm^{-1}$, respectively (Figure 1d).

3.2. XRD analysis

The crystal structure of TiO$_2$, Fe–TiO$_2$ and Pani composite, including 30 wt.% Fe–TiO$_2$, were evaluated using X-Ray diffraction. XRD spectra of pure TiO$_2$ and iron doped TiO$_2$ exhibited a series of distinct diffraction peaks, an indicator of high crystallinity (Figure 2). According to XRD spectra of TiO$_2$ and Fe–TiO$_2$, anatase seems to be the major phase.[30] XRD spectrum of Fe–TiO$_2$ did not contain any characteristic crystalline peak of iron possibly because of the low quantity of the dopant atom. In addition, the other reason might be the similarity of the iron ion (Fe^{3+}) diameter to that of the titanium ion (Ti^{4+}) diameter, which might lead to integration iron ions into TiO$_2$ crystal structure instead of titanium ions. [24] Figure 2a illustrates the diffraction peaks of undoped TiO$_2$ at the angles 25.33°, 37.64°, 47.92°, 53.74°, 55.02°, 62.46° and 68.54°, which were attributed to the (101), (004), (200), (105), (211), (204) and (116) planes, respectively.[24,27] XRD spectrum of Fe–TiO$_2$ did not exhibit any change in the tetraganol crystal structure of undoped TiO$_2$ (Figure 2b). All the XRD peaks agreed with the tetragonal lattice structure. There were only slight changes in position and intensity of the peaks with iron doping, which might be due the substitution of titanium ions by iron ions in TiO$_2$ crystal lattice.[27] Average crystallite size of TiO$_2$ nanoparticles, calculated using the Debye-Scherrer equation on the diffraction peak (101), increased from 19 nm to 20 nm with iron doping.[27] For Fe–TiO$_2$, the slight change in the average crystallite size revealed that the integration of iron ions into TiO$_2$ crystal did not distort the lattice structure too much. XRD spectrum of Pani/Fe–TiO$_2$ composite shows mostly the characteristic diffraction peaks of TiO$_2$ and a weak diffraction peak between 17° and 22°, which was attributed to the crystalline form of emeraldine salt of polyaniline (Figure 2c).[31]

3.3. Morphological analyses

The morphology of the samples was evaluated by SEM analysis. SEM images of TiO$_2$ and Fe–TiO$_2$ illustrate spherical
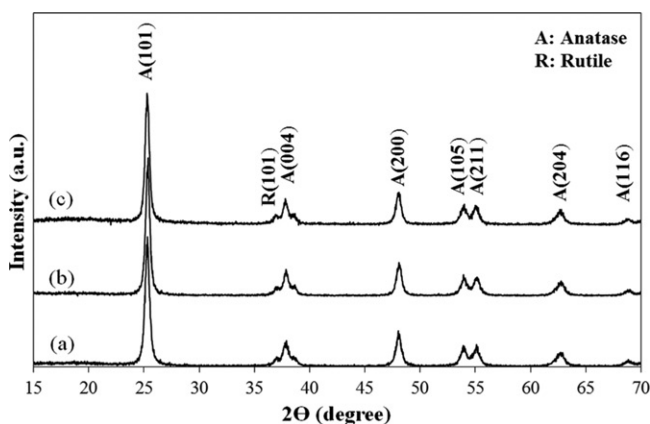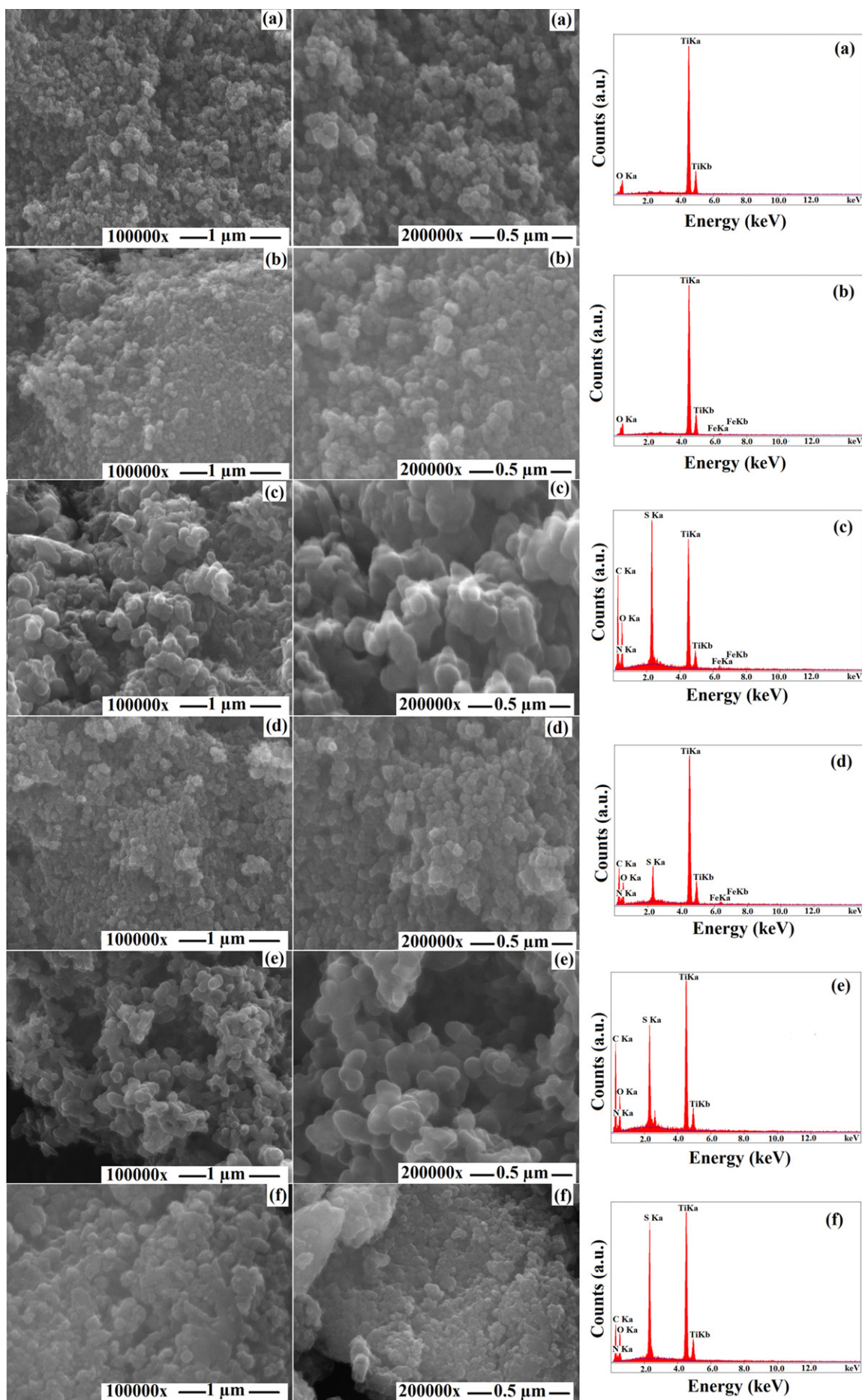

Figure 2. XRD spectra of (a) TiO$_2$, (b) Fe–TiO$_2$ and (c) Pani/Fe–TiO$_2$ (30 wt.%).

Table 1. The discoloration rate of methylene blue for TiO$_2$, Fe–TiO$_2$, pure Pani, Pani/TiO$_2$ composites and Pani/Fe–TiO$_2$ composites.

Sample	k (min^{-1})	R^2
TiO$_2$	0.0012	0.9338
Fe–TiO$_2$	0.0015	0.9718
Pani	0.0003	0.8512
Pani/TiO$_2$ (10 wt.%)	0.001	0.9571
Pani/TiO$_2$ (20 wt.%)	0.0018	0.9515
Pani/TiO$_2$ (30 wt.%)	0.002	0.948
Pani/Fe–TiO$_2$ (10 wt.%)	0.0014	0.9718
Pani/Fe–TiO$_2$ (20 wt.%)	0.0021	0.8176
Pani/Fe–TiO$_2$ (30 wt.%)	0.0025	0.8169

shaped crystallites with aggregation and the aggregates range from 30 nm to 300 nm (Figures 3a and 3b). The crystallite size of the photocatalyst nanoparticles (TiO$_2$ and Fe–TiO$_2$), calculated by Debye-Scherrer's equation, was considerably smaller than the particle size, estimated from SEM images. According to SEM images, iron doping had no significant effect on the morphology of the photocatalyst probably due to low quantity of iron dopant. TiO$_2$ still retained its nanosphere structure. SEM images of Pani/TiO$_2$ and Pani/Fe–TiO$_2$ composites illustrate spherical agglomerate structures, ranging from 100 nm to 1000 nm (Figures 3c-3f). Probably, polyaniline encapsulated the photocatalyst nanoparticles to form the composite structure. As the photocatalyst content of the composites increased from 10 to 30 wt.%, the agglomerates became smaller probably due to the low amount of polyaniline encapsulating the photocatalyst nanoparticles. TiO$_2$ and Fe–TiO$_2$ nanoparticles seem to be uniformly dispersed in polyaniline matrix. The co-ordination interaction of the vacant d orbital of titanium atoms with the lone pair electrons of nitrogen atoms on polyaniline chains might lead to the uniform dispersion of the photocatalyst nanoparticles in polyaniline matrix.[32]

EDX analyses revealed quantitative and qualitative information about chemical composition of the samples. Figure 3 exhibits the EDX spectra of the samples and the quantitative elementel composition of the samples is summarized in Table S1. The EDX spectrum of Fe–TiO$_2$ proved the presence of iron ions within TiO$_2$ structure. Fe/TiO$_2$ weight ratio, obtained by EDX analysis, was comparable to the experimentel ratio. On the other hand, the EDX spectrum of Pani/Fe–TiO$_2$ and Pani/TiO$_2$ composites revealed the presence of the photocatalyst nanoparticles in Pani matrix.

Figure 3. SEM images and EDX spectra of (a) TiO$_2$, (b) Fe–TiO$_2$, (c) Pani/Fe–TiO$_2$ (10 wt.%), (d) Pani/Fe–TiO$_2$ (30 wt.%), (e) Pani/TiO$_2$ (10 wt.%) and (f) Pani/TiO$_2$ (30 wt.%).
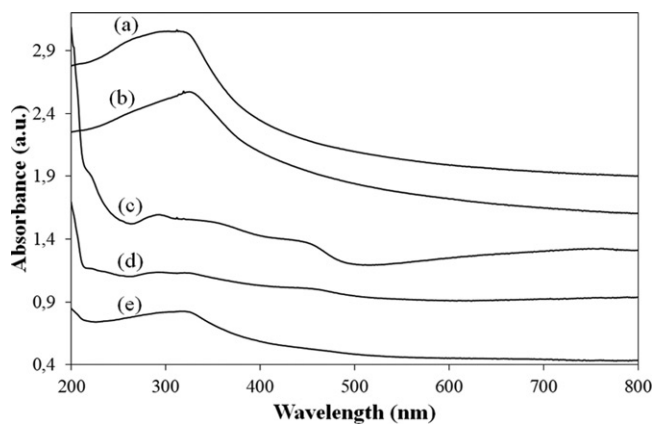
Figure 4. UV–Vis absorbance spectra of (a) Fe–TiO$_2$, (b) TiO$_2$, (c) Pani, (d) Pani/TiO$_2$ (30 wt.%) and (e) Pani/Fe–TiO$_2$ (30 wt.%).

3.4. UV–Vis spectroscopy

UV–Vis spectroscopy was performed to characterize TiO$_2$, Fe–TiO$_2$, pure Pani and the composites. According to Figure 4, TiO$_2$ and Fe–TiO$_2$ absorbed the majority of the incoming light at around 300 nm. Both samples exhibited a typical absorption with an intense transition in the UV region, which was attributed to the intrinsic band gap absorption of TiO$_2$ electrons from the valence band to the conduction band.[33] Unlike TiO$_2$ and Fe–TiO$_2$, Pani absorbed the majority of the incoming light below 500 nm (Figure 4c). Polyaniline extended the absorption of the photocatalyst to the visible light region (400 nm–700 nm), which slightly enhanced the photocalatytic performance of TiO$_2$ within Pani matrix (Figure 4d and e).[34] Since UVC lamp was used as the light source for the removal of the methylene blue, the improvement in photocatalytic activity
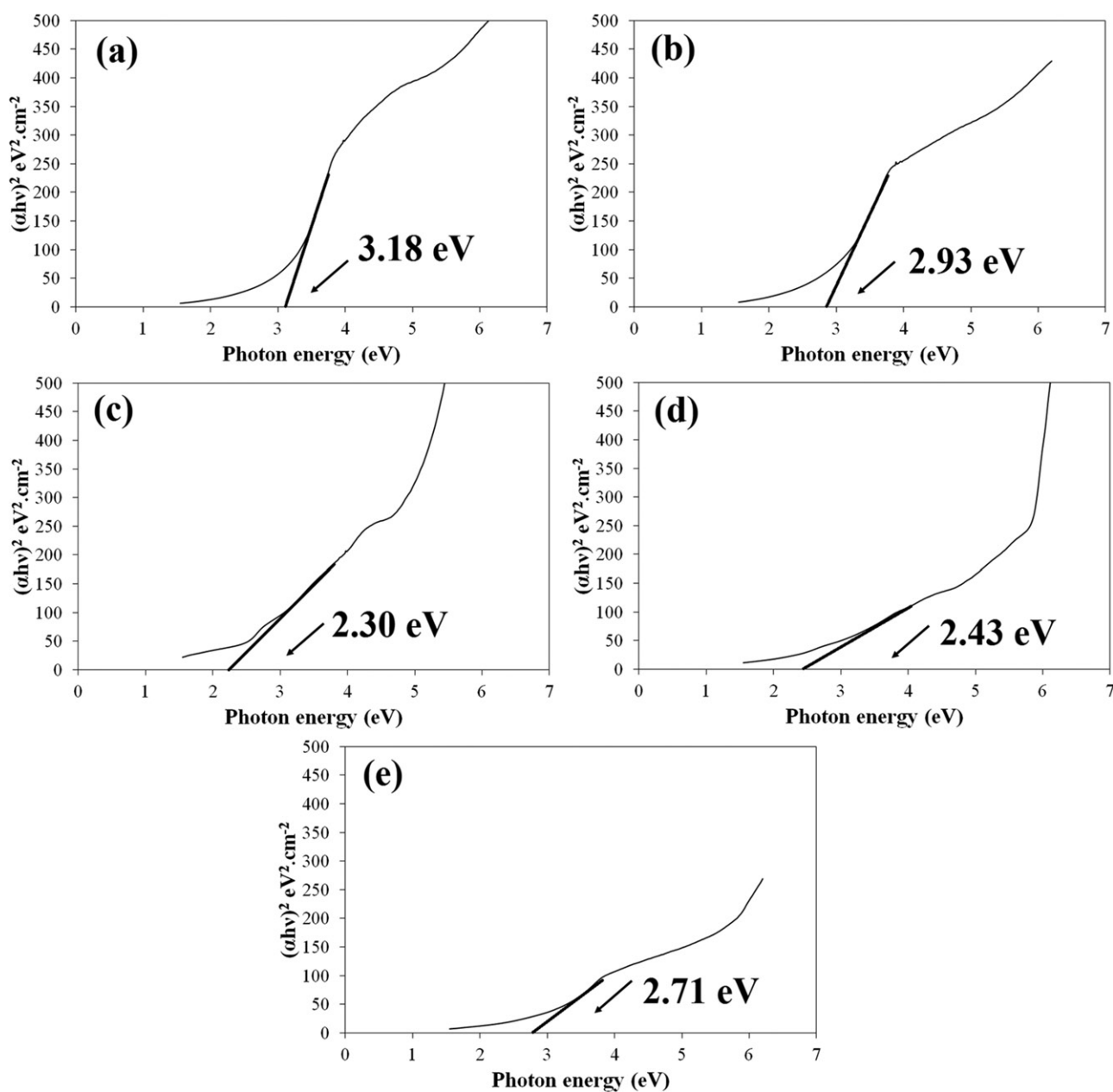

Figure 5. Tauc's plot for (a) Fe–TiO$_2$, (b) TiO$_2$, (c) Pani, (d) Pani/TiO$_2$ (30 wt.%) and (e) Pani/Fe–TiO$_2$ (30 wt.%).

remained limited. UV–Vis spectrum of pure Pani exhibits a characteristic absorption band between 250 nm and 350 nm, which was attributed to π–π^* band transition of the benzenoid structures.[21] Another characteristic peak of Pani related to π band-polaron band of protonated Pani can be seen at 440 nm.[21] UV–Vis spectrum of TiO_2 is shown in Figure 4b. The broad absorption band at around 320 nm was attributed to the characteristic Ti–O–Ti stretching vibrations.[21] Similar to the result in FTIR analysis, the absorption band related to Ti–O–Ti stretching moved towards the lower wavelength due to iron doping (Figure 4a). UV–Vis spectra of the composites resemble to the spectrum of TiO_2 and pure Pani (Figure 4d and e).

The band gap of the samples was estimated through the Tauc's plot analysis of UV–Vis data using the following relation:[35,36]

$$\alpha h\upsilon = A\left(h\upsilon - E_g\right)^{1/2} \qquad (1)$$

Where A is a constant, α is the absorption coefficent, E_g is the band gap and $h\upsilon$ is the photon energy. The Tauc's plot was drawn between $h\upsilon$ vs. $(\alpha h\upsilon)^2$ and the plot was extrapolated to $(\alpha h\upsilon)^2=0$ to estimate the band gap (Figure 5).[35,36] The band gap values for TiO_2, $Fe–TiO_2$, pure Pani, Pani/TiO_2 and Pani/$Fe–TiO_2$ are 2.93 eV, 3.18 eV, 2.30 eV, 2.43 eV and 2.71 eV, respectively. The band gap of TiO_2 widened to 3.18 eV with iron doping and approached to the UVC light region (4.4–12.4 eV), which was significant in terms of the efficiency of the photocatalytic activity. Hence, iron doped TiO_2 could benefit more from UVC light irradiation, which led to the enhanced photocatalytic activity with iron doping. The band gap value of Pani/TiO_2 and Pani/$Fe–TiO_2$ composites varied between the pure polymer and the photocatalyst. As expected, the band gap of Pani/$Fe–TiO_2$ was wider than that of Pani/TiO_2 due to iron doping.

3.5. Photocatalytic activity

Figure 6 shows the variation in the UV–visible spectrum of the dye solution including the samples. Besides, methylene blue removal using TiO_2, Pani, Pani/TiO_2 and Pani/$Fe–TiO_2$ systems is illustrated in Figure 7a and b. Pure Pani provided almost 4% methylene blue degradation after 150 minutes of UV light irradiation. Insignificant removal of methlene blue achieved with pure Pani can be ascribed to low light harvesting efficiency of the conducting polymer.[37] Pure TiO_2 exhibited nearly 15% methylene blue degradation in 150 minutes. In addition, Pani composites with 10 wt.%, 20 wt.% and 30 wt.% of TiO_2 nanoparticles achieved 13%, 21% and 23% methylene blue degradation, respectively, after 150 minutes. When compared with pure photocatalyst, Pani/TiO_2 composites exhibited enhanced photocatalytic activity. Combining the photocatalyst with polyaniline has the potential to improve the photocatalytic activity through hindering the recombination of the photoinduced charge carriers.[38] As a conducting polymer, polyaniline might form transfer channels for photoinduced holes and electrons, which led to a reduced rate of recombination of photoinduced charge
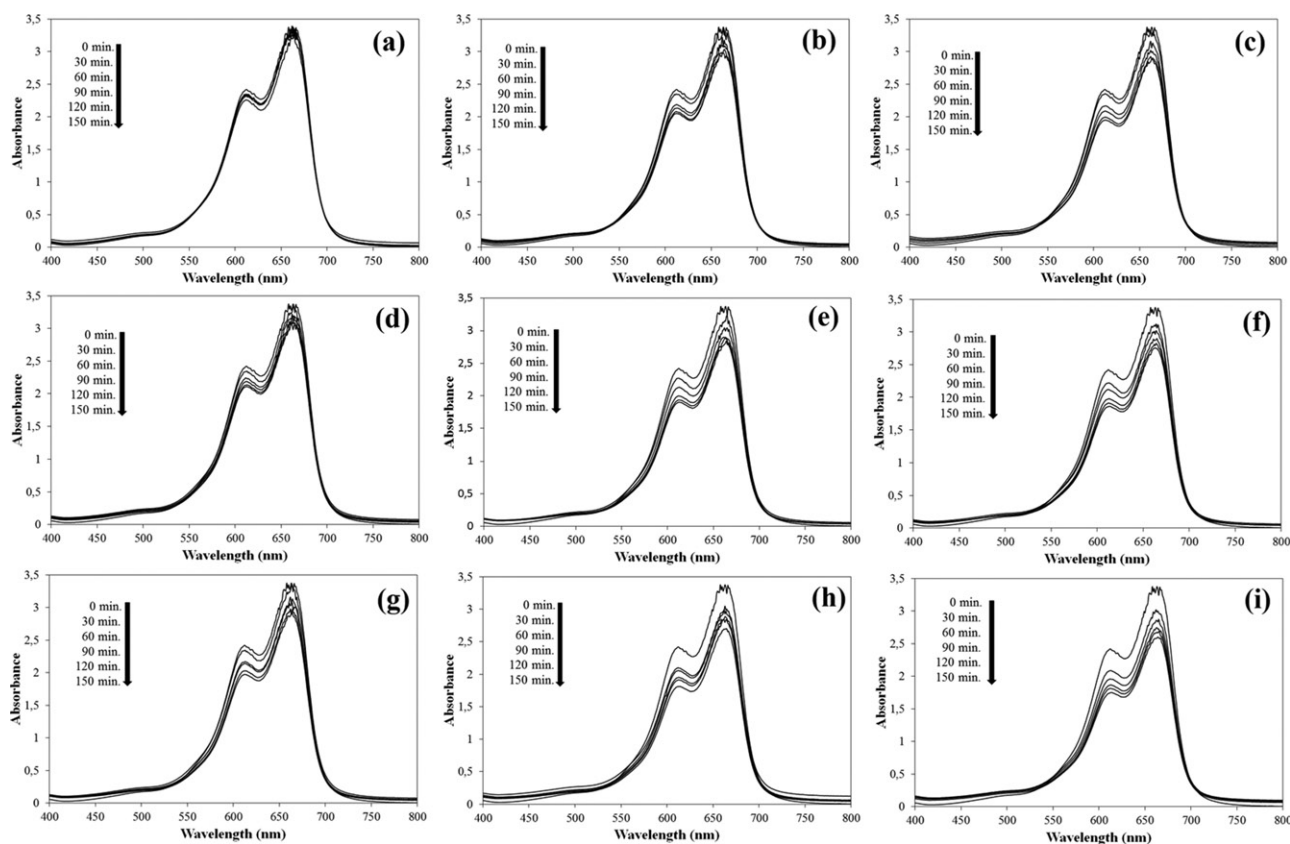

Figure 6. The variation in the UV–visible spectrum of the dye solution including (a) Pani, (b) TiO_2, (c) $Fe–TiO_2$, (d) Pani/TiO_2 (10 wt.%), (e) Pani/TiO_2 (20 wt.%), (f) Pani/TiO_2 (30 wt.%), (g) Pani/$Fe–TiO_2$ (10 wt.%), (h) Pani/$Fe–TiO_2$ (20 wt.%) and (i) Pani/$Fe–TiO_2$ (30 wt.%).
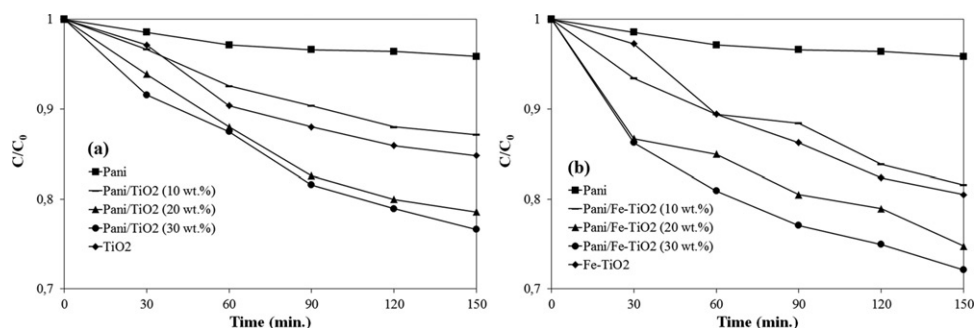
Figure 7. Degradation efficiency of methylene blue over (a) Pani, TiO$_2$ and Pani/TiO$_2$ composites, (b) Pani, Fe–TiO$_2$ and Pani/ Fe–TiO$_2$ composites under UV light irradiation.
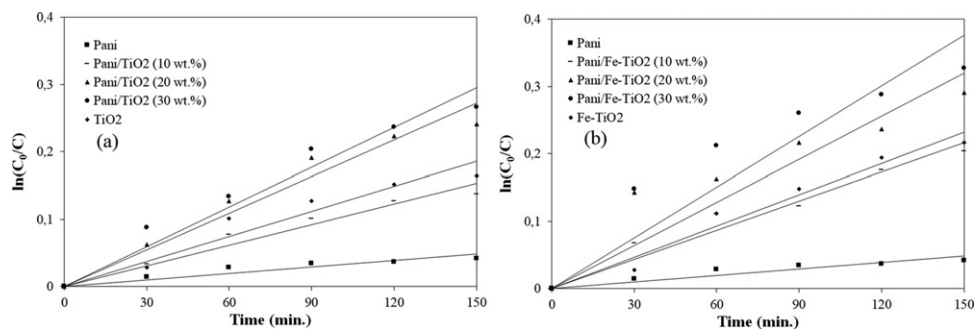
Figure 8. Kinetic plot of degradation reaction of methylene blue over (a) Pani, TiO$_2$ and Pani/TiO$_2$ composites, (b) Pani, Fe–TiO$_2$ and Pani/Fe–TiO$_2$ composites under UV light irradiation.

carriers.[39] The synergic contribution of the conducting polymer and the photocatalyst nanoparticles improved the photocatalytic activity of the composites compared to pure TiO$_2$. Increasing TiO$_2$ content of the composite also enhanced the photocatalytic activity. In addition to the conducting polymer application, iron doping was applied to the photocatalyst to suppress the recombination of the photoinduced holes and electrons through separating the mobile charge carriers, which led to an increases in the efficiency of the photocatalytic activity.[9] Fe–TiO$_2$ nanoparticles exhibited more photocatalytic activity than undoped TiO$_2$. Fe–TiO$_2$ nanoparticles showed almost 19% dye degradation. In the same way, Pani/Fe–TiO$_2$ composites showed more photocatalytic activity than Pani/TiO$_2$ systems at the same compositions. Pani/Fe–TiO$_2$ composites with 10 wt.%, 20 wt.% and 30 wt.% of TiO$_2$ nanoparticles achieved 20%, 25% and 28% dye removal, respectively, which was attributed to the dopant Fe ions hindering the recombination of the photoinduced charge carriers, thereby enhancing the photocatalytic activity.

The reaction kinetics of photodegradation of methylene blue over TiO$_2$, Fe–TiO$_2$, pure Pani, Pani/TiO$_2$ composites and Pani/Fe–TiO$_2$ composites was evaluated using the following pseudo-first order kinetics equation:[40]

$$\ln\left(C_0/C_t\right) \; = kt \qquad (2)$$

Where C_0 and C_t are the concentration of methylene blue initially and after treatment, t is the time and k is the apparent rate constant, determined from the slope of the plot of $\ln(C_0/Ct)$ vs. treatment time t (Figure 8). The discoloration rate of methylene blue for the samples is illustrated on Table 1. The rate of discoloration increased when Pani was combined with TiO$_2$ and Fe–TiO$_2$, respectively. Besides, iron doping enhanced the discoloration rate of the photocatalyst and its composite with Pani. According to high R^2 values close to 1, the reaction kinetics of photodegration of methylene blue over the samples seems to be fit the pseudo-first order kinetics model.[39]

4. Conclusions

Fe-doped TiO$_2$ was successfully prepared using the wet impregnation method and Fe–TiO$_2$ nanoparticles were combined with Pani by in situ polymerization method. XRD pattern of undoped TiO$_2$ and Fe–TiO$_2$ agreed with the tetragonal lattice structure. XRD spectrum of Fe–TiO$_2$ exhibited slight changes in position and intensity of the peaks with iron doping. Besides, the crystallite size of TiO$_2$, calculated by the Debye-Scherrer equation, did not exhibit a significant change with iron doping. According to SEM analysis, TiO$_2$ and Fe–TiO$_2$ illustrated spherical shaped crystallites in aggregate form ranging from 30 nm to 300 nm. Iron doping had no significant effect on the morphology of TiO$_2$ because of low quantity of iron dopant. Besides, the photocatalyst nanoparticles were uniformly dispersed within polyaniline matrix. FTIR and EDX analyses proved that iron ions were integrated into TiO$_2$ crystal structure. In addition, UV–Vis spectroscopy revealed that iron doping widened the band gap of the photocatalyst and approached to the UVC light region. Fe-doped TiO$_2$ and its composites illustrated a considerable improvement in photocatalytic activity for the degradation of methylene blue under UV light irradiation, which was ascribed to iron ions suppressing the recombination of the photogenerated charge carriers.

Funding

References

[1] Fernandez, C.; Larrechi, M. S.; Callao, M. P. An Analytical Overview of Processes for Removing Organic Dyes from Wastewater Effluents. *Trac-Trend. Anal. Chem.* **2010**, *29*, 1202–1211. DOI: 10.1016/j.trac.2010.07.011.

[2] Zhu, T.; Chen, J. S.; Lou, X. W. D. Highly Efficient Removal of Organic Dyes from Waste Water Using Hierarchical NiO Spheres with High Surface Area. *J. Phys. Chem. C* **2012**, *116*, 6873–6878. DOI: 10.1021/jp300224s.

[3] Zangeneh, H.; Zinatizadeh, A. A. L.; Habibi, M.; Akia, M.; Isa, M. H. Photocatalytic Oxidation of Organic Dyes and Pollutants in Wastewater Using Different Modified Titanium Dioxides: A Comparative Review. *J. Ind. Eng. Chem.* **2015**, *26*, 1–36. DOI: 10.1016/j.jiec.2014.10.043.

[4] Barakat, M. A.; Kumar, R. Photocatalytic Activity Enhancement of Titanium Dioxide Nanoparticles: Degradation of Pollutants in Wastewater. In *SpringerBriefs in Green Chemistry for Sustainability*, Sharma, S. K., Ed.; Springer: New York, **2016**.; pp 1–23.

[5] Wang, X.; Feng, X.; Shang, J. Efficient Photoelectrochemical Oxidation of Rhodamine B on Metal Electrodes without Photocatalyst or Supporting Electrolyte. *Front. Environ. Sci. Eng.* **2018**, *12*, 1–6. DOI: 10.1007/s11783-018-1061-8.

[6] Gnaser, H.; Huber, B.; Ziegler, C. Nanocrystalline TiO2 for Photocatalysis. In *Encyclopedia of Nanoscience and Nanotechnology*, Nalwa, H. S., Ed.; American Scientific Publishers: USA, **2004**; Vol. 6, pp 505–535.

[7] Makal, P.; Das, D. Self-doped TiO2 Nanowires in TiO2-B Single Phase, TiO2-B/anatase and TiO2-anatase/rutile Heterojunctions Demonstrating Individual Superiority in Photocatalytic Activity under Visible and UV Light. *Appl. Surf. Sci.* **2018**, *455*, 1106–1115. DOI: 10.1016/j.apsusc.2018.06.055.

[8] Mobtaker, H. G.; Yousefi, T.; Arabieh, M. Enhancing the Photocatalytic Activity of Nano Nd-TiO2@SiO2 by Coupled Systems. *J. Nanostruct.* **2018**, *8*, 31–36. DOI: 10.22052/JNS.2018.01.004.

[9] Sreedhar, M.; Reddy, I. N.; Reddy, C. V.; Shim, J.; Brijitta, J. Highly Photostable Zn-doped TiO2 Thin Film Nanostructures for Enhanced Dye Degradation Deposited by Sputtering Method. *Mat. Sci. Semicon. Proc.* **2018**, *85*, 113–121. DOI: 10.1016/j.mssp.2018.06.005.

[10] Junlabhut, P.; Wattanawikkam, C.; Mekprasart, W.; Pecharapa, W. Effect of Metal (Mn, Co, Zn, Ni) Doping on Structural, Optical and Photocatalytic Properties of TiO_2 Nanoparticles Prepared by Sonochemical Method. *J. Nanosci. Nanotechnol.* **2018**, *18*, 7302–7309. DOI: 10.1166/jnn.2018.15717.

[11] Duan, Z.; Zhu, Y.; Ren, P. R.; Jia, J.; Yang, S.; Zhao, G.; Xie, Y.; Zhang, J. Non-UV Activated Superhydrophilicity of Patterned Fe-doped TiO2 Film for Anti-Fogging and Photocatalysis. *Appl. Surf. Sci.* **2018**, *452*, 165–173. DOI: 10.1016/j.apsusc.2018.05.029.

[12] Unwiset, P.; Makdee, A.; Chanapattharapol, K. C.; Kidkhunthod, P. Effect of Cu Addition on TiO2 Surface Properties and Photocatalytic Performance: X-ray Absorption Spectroscopy Analysis. *J. Phys. Chem. Solids* **2018**, *120*, 231–240. DOI: 10.1016/j.jpcs.2018.05.003.

[13] Ali, I.; Kim, J. O. Visible-light-assisted Photocatalytic Activity of bismuth-TiO2 Nanotube Composites for Chromium Reduction and Dye Degradation. *Chemosphere* **2018**, *207*, 285–292. DOI: 10.1016/j.chemosphere.2018.05.075.

[14] Zhang, C.; Liu, Y.; Zhou, J.; Jin, W.; Chen, W. Tunability of Photo-catalytic Selectivity of B-doped Anatase TiO2 Microspheres in the Visible Light. *Dyes Pigm.* **2018**, *156*, 213–218. DOI: 10.1016/j.dyepig.2018.04.011..

[15] Ren, K.; Gan, Y. X.; Young, T. C.; Moutassem, Z. M.; Zhang, L. Photoelectrochemical Responses of Doped and Coated Titanium Dioxide Composite Nanotube Anodes. *Compos. Part B-Eng.* **2013**, *52*, 292–302. DOI: 10.1016/j.compositesb.2013.04.001.

[16] Gilja, V.; Novakovic, K.; Travas-Sejdic, J.; Hrnjak-Murgic, Z.; Rokovic, M. K.; Zic, M. Stability and Synergistic Effect of Polyaniline/TiO2 Photocatalysts in Degradation of Azo Dye in Wastewater. *Nanomaterials* **2017**, *7*, 1–16. DOI: 10.3390/nano7120412.

[17] Li, Q.; Zhang, C.; Li, J. Photocatalytic and Microwave Absorbing Properties of Polypyrrole/Fe-doped TiO2 Composite by in Situ Polymerization Method. *J. Alloy. Compd.* **2011**, *509*, 1953–1957. DOI: 10.1016/j.jallcom.2010.10.099.

[18] Katancic, Z.; Gavran, I.; Smolkovic, J.; Hrnjak-Murgic, Z. Fly Ash Supported Photocatalytic Nanocomposite Poly(3,4-ethylenedioxythiophene)/TiO2 for Azo Dye Removal under Simulated Solar Irradiation. *J. Appl. Polym. Sci.* **2018**, *35*, 1–12. DOI: 10.1002/app.46316.

[19] Faisal, M.; Harraz, F. A.; Ismail, A. A.; El-Toni, A. M.; Al-Sayari, S. A.; Al-Hajry, A.; Al-Assiri, M. S. Polythiophene/mesoporous SrTiO3 Nanocomposites with Enhanced Photocatalytic Activity under Visible Light. *Sep. Purif. Technol.* **2018**, *190*, 33–44. DOI: 10.1016/j.seppur.2017.08.037.

[20] Yu, X. N.; Lu, Z. Y.; Wu, D.; Yu, P.; He, M.; Chen, T. T.; Shi, W. D.; Huo, P.; Yan, Y. S.; Feng, Y. X. Heteropolyacid-chitosan/TiO2 Composites for the Degradation of Tetracycline Hydrochloride Solution. *React. Kinet. Mech. Cat.* **2014**, *111*, 347–360. DOI: 10.1007/s11144-013-0631-9.

[21] Sarmah, S.; Kumar, A. Photocatalytic Activity of polyaniline-TiO_2 Nanocomposites. *Indian J. Phys.* **2011**, *85*, 713–726. DOI: 10.1007/s12648-011-0071-1.

[22] Dipak, P.; Tiwari, D. C.; Dwivedi, S. K.; Shami, T. C.; Dwivedi, P. K. Synthesis and Characterization Polymer Nanocomposite of PANI/TiO2(np)-Fe + 3 for Microwave Application. *J. Mater. Sci: Mater. Electron.* **2018**, *29*, 6439–6445. DOI: 10.1007/s10854-018-8625-z.

[23] Garg, A.; Singh, A.; Sangal, V. K.; Bajpai, P. K.; Garg, N. Synthesis, characterization and Anticancer Activities of Metal Ions Fe and Cu Doped and co-doped TiO2. *New J. Chem.* **2017**, *41*, 9931–9937. DOI: 10.1039/C7NJ02098H.

[24] Kalantari, K.; Kalbasi, M.; Sohrabi, M.; Royaee, S. J. Enhancing the Photocatalytic Oxidation of Dibenzothiophene Using Visible Light Responsive Fe and N co-doped TiO2 Nanoparticles. *Ceram. Int.* **2017**, *43*, 973–981. DOI: 10.1016/j.ceramint.2016.10.028.

[25] Koysuren, O.; Du, C.; Pan, N.; Bayram, G. Preparation and Comparison of Two Electrodes for Supercapacitors: Pani/CNT/Ni and Pani/Alizarin-Treated Nickel. *J. Appl. Polym. Sci.* **2009**, *113*, 1070–1081. DOI: 10.1002/app.29924.

[26] Koysuren, O.; Koysuren, H. N. Photocatalytic Activity of Polyvinyl Borate/titanium Dioxide Composites for UV Light Degradation of Organic Pollutants. *J. Macromol. Sci. Part A-Pure Appl* **2018**, *55*, 401–407. DOI: 10.1080/10601325.2018.1453259.

[27] Marami, M. B.; Farahmandjou, M.; Khoshnevisan, B. Sol–Gel Synthesis of Fe-Doped TiO_2 Nanocrystals. *J. Electron. Mater.* **2018**, *47*, 3741–3748. DOI: 10.1007/s11664-018-6234-5.

[28] Sahnoun, S.; Boutahala, M. Adsorption Removal of Tartrazine by Chitosan/polyaniline Composite: Kinetics and Equilibrium Studies. *Int. J. Biol. Macromol.* **2018**, *114*, 1345–1353. DOI: 10.1016/j.ijbiomac.2018.02.146.

[29] Bahrudin, N. N.; Nawi, M. A.; Ismail, W. I. N. W. Physical and Adsorptive Characterizations of Immobilized Polyaniline for the Removal of Methyl Orange Dye. *Korean J. Chem. Eng.* **2018**, *35*, 1450–1461. DOI: 10.1007/s11814-018-0052-6.

[30] Kalaiarasi, S.; Jose, M. Streptomycin Loaded TiO2 Nanoparticles: preparation, characterization and Antibacterial

Applications. *J. Nanostruct. Chem.* **2017**, *7*, 47–53. DOI: 10.1007/s40097-016-0213-2.

[31] Cui, S.; Wang, J.; Wang, X. Fabrication and Design of a Toxic Gas Sensor Based on Polyaniline/titanium Dioxide Nanocomposite Film by Layer-by-layer Self-Assembly. *RSC Adv.* **2015**, *5*, 58211–58219. DOI: 10.1039/C5RA06388D.

[32] Ramesan, M. T.; Sampreeth, T. In Situ Synthesis of Polyaniline/Sm-doped TiO2 Nanocomposites: Evaluation of Structural, Morphological, Conductivity Studies and Gas Sensing Applications. *J. Mater. Sci: Mater. Electron.* **2018**, *29*, 4301–4311. DOI: 10.1007/s10854-017-8377-1.

[33] Zarrin, S.; Heshmatpour, F. Photocatalytic Activity of TiO$_2$/Nb$_2$O$_5$/PANI and TiO$_2$/Nb$_2$O$_5$/RGO as New Nanocomposites for Degradation of Organic Pollutants. *J. Hazard. Mater.* **2018**, *351*, 147–159. DOI: 10.1016/j.jhazmat.2018.02.052.

[34] Cui, W.; He, J.; Wang, H.; Hu, J.; Liu, L.; Liang, Y. Polyaniline Hybridization Promotes Photo-electro-catalytic Removal of Organic Contaminants over 3D Network Structure of rGH-PANI/TiO2 Hydrogel. *Appl. Catal. B-Environ.* **2018**, *232*, 232–245. DOI: 10.1016/j.apcatb.2018.03.069.

[35] Tumuluri, A.; Naidu, K. L.; K. C. J. Band, R. Gap Determination Using Tauc's Plot for LiNbO3 Thin Films. *Int. J. ChemTech. Res.* **2014**, *6*, 3353–3356.

[36] Sharma, G.; Bhogal, S.; Naushad, M.; Inamuddin, Kumar, A.; Stadler, F. J. Microwave Assisted Fabrication of La/Cu/Zr/carbon Dots Trimetallic Nanocomposites with Their Adsorptional vs Photocatalytic Efficiency for Remediation of Persistent Organic Pollutants. *J. Photochem. Photobiol. A-Chem.* **2017**, *347*, 235–243. DOI: 10.1016/j.jphotochem.2017.07.001.

[37] Piewnuan, C.; Wootthikanokkhan, J.; Ngaotrakanwiwat, P.; Meeyoo, V.; Chiarakorn, S. Preparation of TiO$_2$/(TiO$_2$−V$_2$O$_5$)/Polypyrrole Nanocomposites and a Study on Catalytic Activities of the Hybrid Materials under UV/Visible Light and in the Dark. *Superlattices Microstruct.* **2014**, *75*, 105–117. DOI: 10.1016/j.spmi.2014.07.026.

[38] Lee, S. Y.; Park, S. J. TiO2 Photocatalyst for Water Treatment Applications. *J. Ind. Eng. Chem.* **2013**, *19*, 1761–1769. DOI: 10.1016/j.jiec.2013.07.012.

[39] Brooms, T. J.; Otieno, B.; Onyango, M. S.; Ochieng, A. Photocatalytic Degradation of P-Cresol Using TiO2/ZnO Hybrid Surface Capped with Polyaniline. *J. Environ. Sci. Health Part A-Toxic/Hazard. Subst. Environ. Eng.* **2018**, *53*, 99–107. DOI: 10.1080/10934529.2017.1377583.

[40] Tanwar, R.; Kumar, S.; Mandal, U. K. Photocatalytic Activity of PANI/Fe-0 Doped BiOCl under Visible Light-degradation of Congo Red Dye. *J. Photochem. Photobiol. A-Chem.* **2017**, *333*, 105–116. DOI: 10.1016/j.jphotochem.2016.10.022.